II

RESEARCH ARTICLES

ENGINEERING CHARACTERIZATION OF STRENGTH AND ELASTIC PROPERTIES OF GEOPOLYMER CEMENT CONCRETE MATERIALS

Brett Tempest[1], Janos Gergely[2] and David C. Weggel[3]

ABSTRACT

Geopolymer cements provide an alternative to the Portland cement used to produce structural concrete. In this study, geopolymer cements were used to create concrete having compressive strength in the range of 34 to 83 MPa (5,000-12,000 psi). The mechanical properties of these concrete materials were evaluated to determine the compressive and tensile strengths and immediate and long term elastic behaviors. The geopolymer cement concrete (GCC) was found to perform in a similar manner to Portland cement concrete (PCC). Long term shrinkage and creep properties of GCC materials were found to be lower than the values typical for PCC.

KEYWORDS

geopolymer, shrinkage, creep, elastic modulus, stress-strain, modulus of rupture

INTRODUCTION

Recent reports have illustrated the rapidly increasing technical readiness of geopolymer based building materials in structural applications. Azarbayjani et al. described the design and construction of a residential building with loadbearing, precast geopolymer cement concrete (GCC) walls (2014). Around the same time, the University of Queensland raised a GCC building to house the Global Change Institute (Johnson, 2014). These projects are significant to the advancement of green building due to their successful application of an innovative cement that can significantly reduce carbon emissions from cement production.

GCC is a low emissions alternative to Portland Cement Concrete (PCC) that can be manufactured from a range of alumina and silica rich source materials which are abundant in the Earth's crust. Materials like clay, as well as industrial combustion byproducts, such as rice husk ash and coal fly ash can be raw materials for geopolymer cement manufacturing. The flexibility of the geopolymerization process allows manufacturers to select locally abundant quantities of alumino-silicate source materials. Often coal fly ash, a waste material originating

1. Brett Tempest is an Assistant Professor of Civil and Environmental Engineering at the University of North Carolina at Charlotte.
2. Janos Gergely is an Associate Professor of Civil and Environmental Engineering at the University of North Carolina at Charlotte.
3. David C. Weggel is a Professor of Civil and Environmental Engineering at the University of North Carolina at Charlotte.

from coal-fueled electricity generation, is a source material of choice due to its abundance and availability around the world.

The process of preparing GCC generally involves mixing the alumino-silicate source materials with a chemical activator consisting of a strong alkaline solution such as caustic soda and waterglass. The fly ash activator mixture is then combined with aggregates, placed in molds, and consolidated much like PCC. Unlike PCC, most GCC formulations require high temperature curing in order to achieve significant strength. Thus, the characteristics of cured GCC relate to a range of variables including the source material properties, the activator composition, and the heating and curing conditions. In this experimental work, the variables, mellowing time, heating time and activator composition were manipulated to determine their impact on compressive strength, tensile strength and modulus of elasticity. A single source of fly ash was maintained throughout this study so as to not introduce additional variables related to ash characteristics.

Mechanism of Geopolymerization

A basic, general model of the geopolymerization process proposed by Glukhovsky is expressed as a series of three reaction phases (Glukhovsky, 1959):

1) Dissolution – the aluminosilicate material is dissolved in an alkaline "activating" solution;
2) Reorientation – the liberated silicate and aluminate monomers form short aluminosilicate oligomers;
3) Solidification – the three dimensional geopolymer matrix becomes rigid.

The initiation of the geopolymerization phases described above is caused by the addition of an activating solution to the source material. The solution contains the alkalinity that causes the dissolution of the source material solids, and sometimes also contains a supplementary source of soluble silicates. The two predominant alkaline salts used in geopolymer formation are NaOH and KOH. Each of these results in slightly different dissolution rates and hardened geopolymer characteristics. Greater dissolution rates for both Si and Al have been found in solutions of NaOH (Fernández-Jiménez and Palomo, 2005, Mikuni, Komatsu and Ikeda, 2007). The impact of the more effective dissolution ability of NaOH solutions is that the equilibrium of dissolved species and undissolved species is reached at lower levels of alkalinity (Panagiotopoulou, Kontori, Perraki and Kakali, 2007).

Comparison of the hardened properties of geopolymers formed with activating solutions containing either K or Na have shown an impact on the compressive strength and durability of the concrete. Van Jaarsveld and van Deventer (1999) demonstrated that potassium activating solutions produced slightly higher compressive strength geopolymers. However, the potassium based activators also produced materials with higher specific surface area and lower resistance to acid attack. The strength of these solutions which lead to structural strength materials (i.e. f'c> 28MPa (4,000 psi)), has ranged from 8 to 16 molar (Diaz-Loya, Allouche and Vaidya, 2011; Hardjito and Rangan, 2005; Sun, 2005).

The dissolution rates of aluminate and silicate species in the activating solution are affected by a combination of thermal conditions and the molarity of the alkaline solution. With both sodium and potassium based activating solutions, dissolution rates are known to increase with increasing alkalinity (Mikuni, Komatsu and Ikeda, 2007; Sagoe-Crentsil and Weng, 2007). However, despite the dissolution capacity of higher alkalinity solutions, the

presence of excessive concentrations of sodium hydroxide have been found to reduce the compressive strength of hardened geopolymer. This is due to the reduced degree of polymerization that is caused by excessive NaOH concentrations. The balance of silicate species at high alkalinity levels tends to favor smaller monomers over the larger oligomers and therefore a lower degree of polycondensation (Panias, Giannopoulou and Perraki, 2007).

Setting time for geopolymer cements can be affected by chemical species in the source materials or by external conditions, such as temperature. In this paper, the mellowing period between mixing and the initiation of high-temperature curing is referred to as aging time. Reorientation of monomers and oligomers occurs during this aging period until the solidification of the concrete begins to limit transport. The rapid gain of strength typically occurs during a period of elevated temperature curing. Temperatures between 60°C and 100°C have been reported at ambient pressures with the general trend of greater strength gain being associated with higher temperatures (Sindhunata, vanDeventer, Lukey and Xu, 2006; van Jaarsveld, van Deventer and Lukey, 2002).

Mechanical Characteristics Examined

In order to encourage further scaled demonstrations of GCC, and ultimately adoption for infrastructure applications, it is important to produce an inventory of research results that characterize mechanical performance and relate it to mix design parameters. Required knowledge includes characterization of the GCC response to compressive and tensile loading, and long-term behavior such as creep and shrinkage. Such results will justify or dissuade the application of existing concrete design guidelines, and will eventually result in specialized provisions for GCC construction.

Creep

The time-dependent deformation of concrete under sustained loads is referred to as creep. In Portland cement concrete, the paste fraction undergoes dimensional changes while hard aggregates tend to restrain creep-related deformation. After concrete cures and enters service, a series of processes that result in volumetric changes occur, including free shrinkage strain ε_{sh}, basic creep ε_{bc}, drying creep ε_{dc}, and elastic strains ε_{e}. The total strain measured in a concrete element is a combination of these constituent strains, as given by

$$\varepsilon_{total} = \varepsilon_{sh} + \varepsilon_{bc} + \varepsilon_{dc} + \varepsilon_{e} \tag{1}$$

The summation of these strains is the total measurable strain. Creep strain, ε_{cr}, is taken as the sum of ε_{bc} and ε_{dc}. The ratio of creep strain, ε_{cr}, to elastic strain, ε_{e}, is known as the creep coefficient, C, as given by

$$C = \frac{\varepsilon_{cr}}{\varepsilon_{e}} \tag{2}$$

The creep coefficient changes over time as the strains attributable to creep processes become similar in magnitude to and then greater than elastic strains. For design purposes, ACI Committee 209 (2008) provides Equation 3 as a means of estimating the creep coefficient at t days, as a function of the ultimate creep, C_u. The ultimate creep coefficient for Portland cement concrete is known to range from 1.30 to 4.15, with an average value of 2.35 (Branson, 1976).

$$C_t = \frac{t^{0.6}}{D+t^{0.6}} C_u \tag{3}$$

where:

C_t: creep coefficient at time, t

t: time (days)

D: constant usually taken as 10 days

C_u: ultimate creep coefficient

The measurement of creep in controlled laboratory settings is undertaken by preparing concrete cylinders, allowing them to cure for a specified period of time, and then subjecting them to a compressive stress that does not exceed the proportional limit for the material. The range typically used is less than 40% of the concrete cylinder's compressive strength. In order to compare the results of tests that were conducted using different stress intensities, the factor, specific creep ϕ, is defined as the ratio between creep strain and applied stress σ. This relationship is given by

$$\phi = \frac{\varepsilon_{cr}}{\sigma} \tag{4}$$

where:

ϕ: specific creep

ε_{cr}: basic plus drying creep strain ($\varepsilon_{bc} + \varepsilon_{dc}$)

σ: applied compressive stress

Shrinkage

Removal of water from the concrete matrix causes shrinkage strains as the overall volume of the monolith is reduced. When the water is removed from fresh concrete, the resulting shrinkage is known as plastic shrinkage. The effects of plastic shrinkage are manifested in crack patterns that negatively impact the appearance and durability of concrete surfaces. In hardened concrete, shrinkage processes are a result of the continued removal of water from the pore system of the concrete either by self-desiccation in autogenous shrinkage, by chemical reaction in carbonation shrinkage, or by evaporation (Mindess, Young and Darwin, 2003).

Predicting the magnitude of shrinkage is important to the design of concrete structures. If the designer can properly locate construction joints and control restraint against shrinkage, cracks can be eliminated or limited to acceptable locations. Passive or prestressing reinforcement is also a design requirement to restrain shrinkage in concrete structures, with minimum steel ratios given by ACI 318 (American Concrete Institute, 2011).

Shrinkage of the concrete of structures in service is a process that involves many variables. These include the duration of wet curing, air content, aggregate characteristics, temperature, and relative humidity around the structure. ACI committee 209 (2008) provides guidelines for estimating shrinkage of concrete after periods of time. Prediction of the magnitude of the shrinkage is made with

$$(\varepsilon_{sh})_t = \frac{t^a}{f + t^a} \; (\varepsilon_{sh})_u \tag{5}$$

where:

$(\varepsilon_{sh})_t$: shrinkage strain at time t

t: time in days

a: power of t (~1.0)

f: constant taken as 20-130 days

$(\varepsilon_{sh})_u$: ultimate shrinkage, 800×10^{-6} mm/mm [in/in]

Although shrinkage can cause serious durability and aesthetic problems in all types of concrete structures, it presents a special concern in prestressed concrete sections. As shrinkage strains increase in the concrete, the elongation of the prestressing steel tendons is reduced, causing a net reduction in the effective prestress. The magnitude of this reduction is related to the modulus of the steel as given by

$$\Delta f_{sh} = \varepsilon_{sh} E_{ps} \tag{6}$$

where:

Δf_{sh}: change in stress in the prestressing steel due to concrete shrinkage

ε_{sh}: shrinkage strain

E_{ps}: modulus of elasticity for prestressing steel, MPa [psi]

This study reports the modulus of elasticity, compressive strength, and tensile strength as necessary inputs to any strength design process. The impacts of some GCC preparation parameters are also assessed.

EXPERIMENTAL INVESTIGATION

The goal of this study was to understand the impact of activator alkalinity level, pre-curing aging time and high temperature curing time on the strength and elastic characteristics of GCC. A series of three concrete mixtures were produced having the composition shown in Table 1. The three GCC mixes were designated as GCC-1, GCC-2 and the PCC mix was designated PCC-1. The creep and shrinkage characteristics of the concrete were measured and compared for mixes, GCC-2 and PCC-1. The batch of GCC-2 specimens selected for shrinkage and creep measurements were from the 48 hours aging and 48 hours curing group as they achieved the most comparable compressive strength to the PCC-1 materials.

TABLE 1. Mixing proportions kg/m³ (lb/yd³)

Material	Mix Designation		
	GCC-1	GCC-2	PCC-1
Portland Cement	0	0	386 (229)
Fly Ash	835 (495)	798 (474)	89 (53)
Water	275 (163)	275 (163)	173 (103)
Sodium Hydroxide	84 (50)	103 (62)	0
Silica Fume	63 (37)	77 (46)	0
Fine Aggregate	1,336 (793)	1,336 (793)	709 (421)
Coarse Aggregate	1,336 (793)	1,336 (793)	1,127 (669)

Materials

Fly ashes were sourced from a southeastern US steam station. The ashes are marketable as Class F and had their oxide analysis determined by X-ray fluorescence described in Table 2. The activating solution consisted of sodium hydroxide pellets combined with silica fume and mixed into the quantity of water shown in Table 1. The activator was equilibrated in a 75°C (167°F) oven for 24 hours immediately prior to mixing the geopolymer cement concrete. Coarse aggregates consisted of 9.5mm (3/8") granite material and fine aggregate silica concrete sand, both gradations being shown in Table 3. Extensive information on the development of these mix designs is described in Tempest (2010).

TABLE 2. XRF analysis of fly ashes.

Oxide	% by Mass
SiO_2	56.20
TiO_2	1.46
Al_2O_3	28.00
Fe_2O_3	5.22
MnO	0.02
MgO	1.00
CaO	1.52
Na_2O	0.21
K_2O	2.74
P_2O_5	0.18
Totals	96.55
LOI	3.32

TABLE 3. Gradation of fine and coarse aggregates in GCC-1 and GCC-2.

Sieve Opening in (mm)	% finer	
	Coarse	Fine
5/8 (16.0)	100	100
1/2 (12.5)	99.50	100
3/8 (9.5)	85.30	99.77
no. 4 (4.75)	28.80	99.54
no. 8 (2.36)	5.50	97.94
no. 16 (1.18)	1.30	90.37
no. 40 (0.425)	0.70	37.16
no. 50 (0.300)	0.70	19.95
no. 100 (0.150)	0.50	1.61
Pan	0	0

Specimens

Specimens were prepared using sampling and consolidation techniques specified in ASTM C192 (2007). Due to the viscous nature of GCC, consolidation was achieved by placing the samples on a vibrating table for two minutes. The specimens were either immediately added to the curing oven or aged at ambient laboratory conditions for 24 or 48 hours. Curing of the GCC samples was at 75°C (167°F) for either 24 or 48 hours. From each batch and curing group, three cylinders were tested in compression in accordance with ASTM C39 (2005), three were tested in splitting according to ASTM C496 (2004), and three were tested for the static modulus of elasticity according to ASTM C469 (2002). The experimental evaluation was carried out on a universal testing machine.

Specimens used for shrinkage and creep evaluation consisted of materials made from GCC-2. These specimens were aged at ambient laboratory conditions for 48 hours and

then cured at 75°C (167°F) for 48 hours. A set of comparison specimens was prepared with PCC having the mix design shown in Table 1. These specimens were cured with procedures described in ASTM C512 (2002) and ASTM C157 (2008), with some modifications that are explained in the section pertaining to shrinkage.

RESULTS AND DISCUSSION

Compressive and Tensile Strength

The compressive and tensile test results are provided in Table 4. As a general rule, the higher alkalinity of the activating solution used in GCC-2 resulted in higher compressive strength. Strength increased when the alkalinity of the activating solution was increased from 10% NaOH/fly ash (GCC-1) to 13% NaOH/fly ash (GCC-2). This increase in compressive strength was most likely due to greater dissolution of the fly ash source material. Greater dissolution leads to more monomers available to generate the geopolymeric binder.

TABLE 4. Strength and elastic test results.

Mix	Aging Time (hours)	Curing Time (hours)	Compressive Strength MPa (psi)	RSD %	Tensile Strength MPa (psi)	RSD %	Modulus Of Elasticity MPa (ksi)	RSD %
GCC-1	0	24	36.6 (5,300)	7.0%	3.25 (475)	14.7%	20,400 (2,950)	9.5%
GCC-1	0	48	41.4 (6,010)	5.6%	3.85 (555)	12.8%	22,600 (3,300)	15.0%
GCC-1	24	24	40.8 (5,910)	2.9%	2.9 (420)	20.2%	20,400 (2,950)	8.4%
GCC-1	24	48	44.6 (6,460)	5.9%	3.75 (545)	7.3%	24,200 (3,500)	4.5%
GCC-1	48	24	40.9 (5,940)	0.9%	3.35 (485)	13.4%	21,800 (3,150)	7.1%
GCC-1	48	48	48.1 (6,980)	5.0%	3.8 (550)	7.3%	22,800 (3,300)	10.1%
GCC-2	0	24	50.7 (7,360)	2.9%	4.9 (710)	22.0%	24,400 (3,550)	5.7%
GCC-2	0	48	55 (7,980)	29.9%	5.25 (765)	4.7%	23,800 (3,450)	1.4%
GCC-2	24	24	53.3 (7,730)	2.3%	3.8 (555)	3.8%	24,400 (3,550)	4.6%
GCC-2	24	48	64.2 (9,310)	3.9%	4.8 (695)	2.2%	28,600 (4,150)	0.2%
GCC-2	48	24	57.1 (8,290)	3.4%	6.05 (880)	12.3%	26,200 (3,800)	3.6%
GCC-2	48	48	67.5 (9,790)	2.2%	5.85 (850)	13.6%	28,800 (4,200)	2.1%

RSD:relative standard deviation

Longer aging and curing times yielded greater strength. Increased aging time from 0 to 48 hours improved the 28-day compressive strength in all cases. Increased curing time at 75⁰ C (167⁰ F) also improved the 28 day strength in each of the mixes. In specimens produced with the GCC-1 mix, 75⁰ C (167⁰ F) curing for an additional 24 hours increased the compressive strength by an average of 12%. The effect of aging the GCC-1 specimens for an additional 24 hours was a 6% increase in compressive strength. Specimens prepared with the GCC-2 mix design, showed an average compressive strength increase of 13% due to an additional 24 hours of curing at 75⁰ C (167⁰ F). An additional 24 hours of room temperature aging increased compressive strength by 8% on average. Thus, for both GCC-1 and GCC-2, the impact of additional curing time to increased compressive strength was greater than the impact of additional aging time. The positive influence of longer curing time has been already documented (Hardjito and Rangan, 2005); however, the magnitude of the benefits from extended aging was unexpected, but was also most likely related to greater dissolution rates and the opportunity for transport and reorientation before the matrix solidified.

As with Portland cement concrete, the split cylinder tensile strength of the geopolymer cement concrete specimens was found to be proportional to the compressive strength. Table 4 shows that the tensile strength ranged from 7.10% to 10.6% of the compressive strength. The results shown in Table 4 are plotted in Figure 1. Large numbers of test results on PCC compressive and split cylinder tests have revealed an average tensile strength, f_{ct}, of (Wight, Richart and MacGregor, 2012):

$$f'_{ct} = 0.53\sqrt{f'_c} \text{ [MPa]} \quad (7)$$

$$f'_{ct} = 6.4\sqrt{f'_c} \text{ [psi]} \quad (8)$$

where:

f_{ct}: concrete cylinder splitting strength,

f_{ct}: concrete cylinder compressive strength.

Similar to PCC, Figure 1 shows a strong relationship between the tensile and compressive strength of GCC-1 and GCC-2 cylinders. The corresponding equations for GCC are given in Equation 9 and 10, showing that the GCC tested in this research was slightly more efficient in resisting tensile stresses than would be predicted by the index Equations given as 7 and 8. The regression line given by Equation 9 and 10 and shown in Figure 1 represents the data with correlation coefficient, R^2=0.84.

$$f'_{ct} = 0.616\sqrt{f'_c} \text{ [MPa]} \quad (9)$$

$$f'_{ct} = 7.4\sqrt{f'_c} \text{ [psi]} \quad (10)$$

Figure 1: Relationship between splitting tensile and compressive strength of GCC and regression line given by Equations 9 and 10.

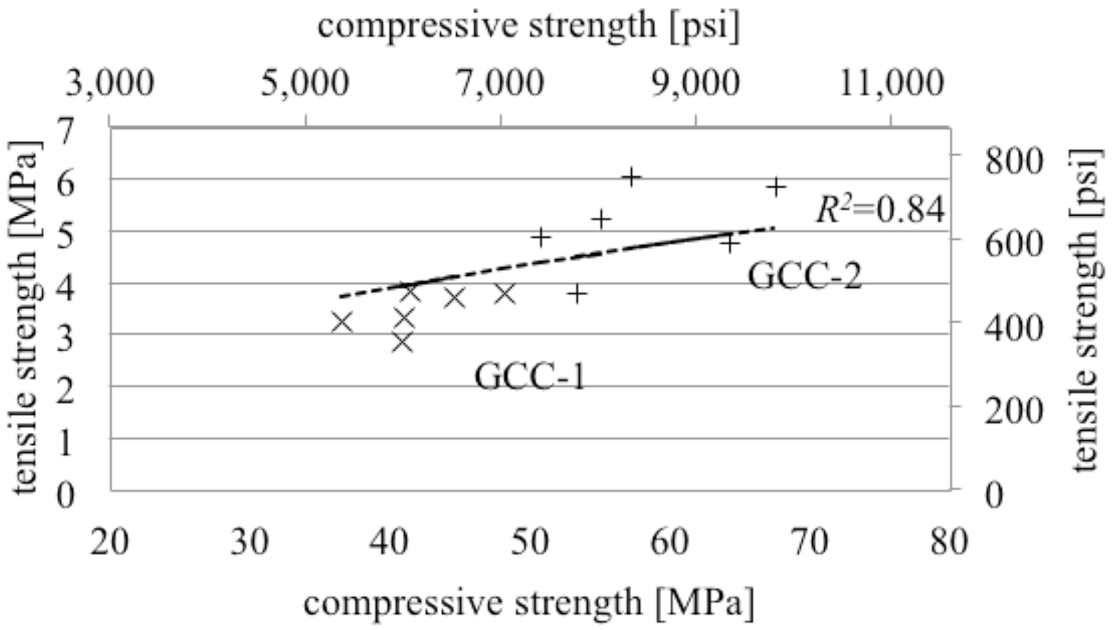

Figure 2: Relationship between modulus of elasticity and compressive strength of GCC and regression line given by Equations 15 and 16.

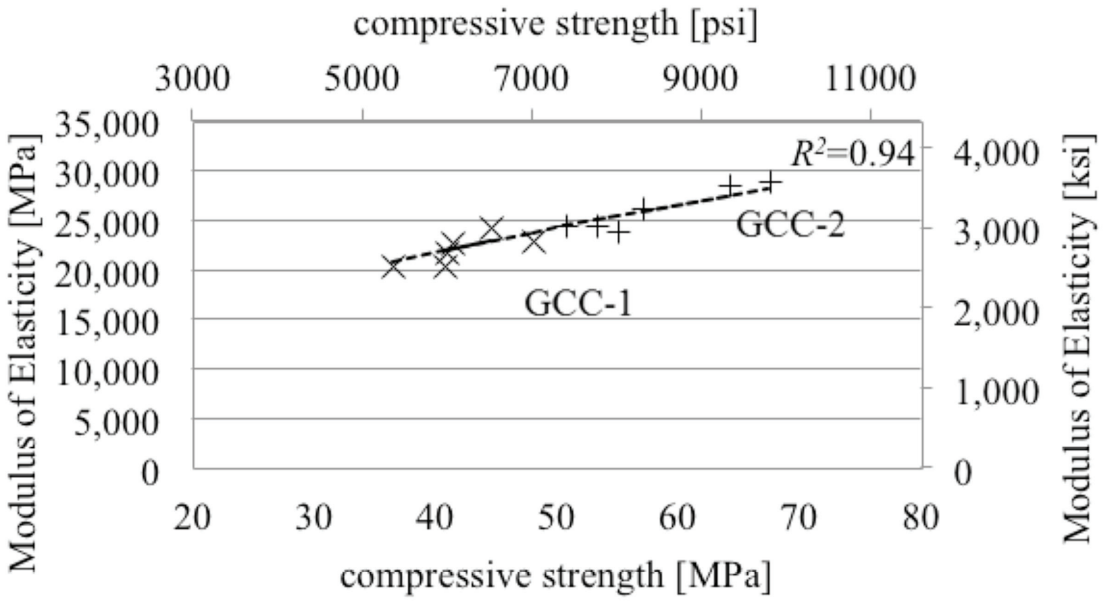

Modulus of Elasticity

The modulus of elasticity of the concrete was measured using the procedure given in ASTM C469 (ASTM, 2002a). The results given in Table 4 are plotted in Figure 2, and show a clear trend towards increasing modulus with increasing compressive strength. It is typical in concrete design to estimate the modulus of elasticity of Portland cement concrete by relating it to the specified compressive strength and the unit weight using Equations 11 and 12 (ACI, 2011).

$$E_c = w_c^{1.5} * 0.043\sqrt{f_c'} \quad \text{[MPa]} \tag{11}$$

$$E_c = w_c^{1.5} * 33\sqrt{f_c'} \quad \text{[psi]} \tag{12}$$

where:

E_c: modulus of elasticity of concrete,

w_c: unit weight of concrete.

For normal-weight concrete, having density of 2,307 kg/m^3 (144 lb/ft^3), Equations 11 and 12 become

$$E_c = 4{,}730\sqrt{f_c'} \quad \text{[MPa]} \tag{13}$$

$$E_c = 57{,}000\sqrt{f_c'} \quad \text{[psi]} \tag{14}$$

The unit weight of the geopolymer cement concrete produced in this study was found to be 2,243 kg/m^3 (140 lb/ft^3). However, because all the concrete produced in this study had essentially the same unit weight, there is no basis to use the unit weight as a predictor of GCC modulus of elasticity. More data would be required to make such correlations. The relationship between cylinder compressive strength and modulus of elasticity found for the materials produced in this study is given by Equations 15 and 16, respectively, showing a lower modulus than PCC for a given compressive strength for GCC. The regression line given by Equations 15 and 16 has a correlation coefficient, R^2=0.94, with the experimental data.

$$E_c = 3{,}421\sqrt{f_c'} \quad \text{[MPa]} \tag{15}$$

$$E_c = 41{,}193\sqrt{f_c'} \quad \text{[psi]} \tag{16}$$

Creep Measurement

Other than the provision of high-temperature curing for the GCC specimens, the preparation of the GCC and PCC specimens was the same. All specimens, GCC and PCC, were initially loaded at an age of 28 days with a common load of 156 kN (35,000 lb). This corresponds to a compressive stress on the cylinder of 8.5 MPa (1,238 psi). The cylinders were capped with a sulfur compound and loaded in pairs into the frame shown in Figure 3. Strain measurements were made with a demountable mechanical strain gage at the time intervals specified in ASTM C512 (2002). Strains were measured at two points along opposite sides of each specimen. These strains were then averaged over the two specimens that were prepared

for each mix. The strains of the loaded specimens were reduced by the average strain found in the unloaded specimens in order to eliminate shrinkage strains from the measurements. The 28-day compressive strength of the concrete materials used in these specimens is given in Table 5.

Figure 3: Creep specimen loading apparatus.

TABLE 5. Compressive strength and initial elastic modulus of creep specimens.

Concrete	28-day f'_c MPa (psi)	E_i GPa (psi)
GCC 2	65.5 (9,500)	19.6 (2,842,271)
PCC-1	77.2 (11,200)	35.6 (5,170,922)

Figures 4 and 5 show the relationship of creep strain with total strain for the GCC and PCC specimens, respectively. The concrete materials produced the expected hyperbolic curve relating creep strains with time. Included in the total strain are elastic strains, shrinkage strains and creep strains. It is apparent that both the total strain and the creep strain were larger in magnitude for the PCC specimens despite their having a much higher initial elastic modulus.

Figure 4: Relationship of creep strain with time for GCC-2 specimens.

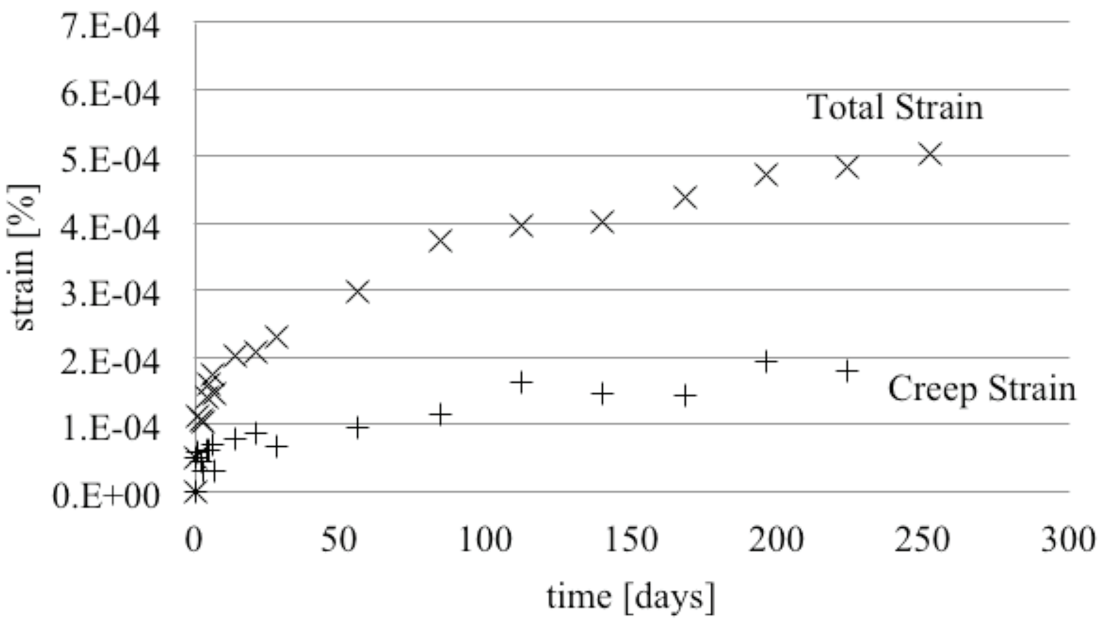

Figure 5: Relationship of creep strain with time for PCC-1 specimens.

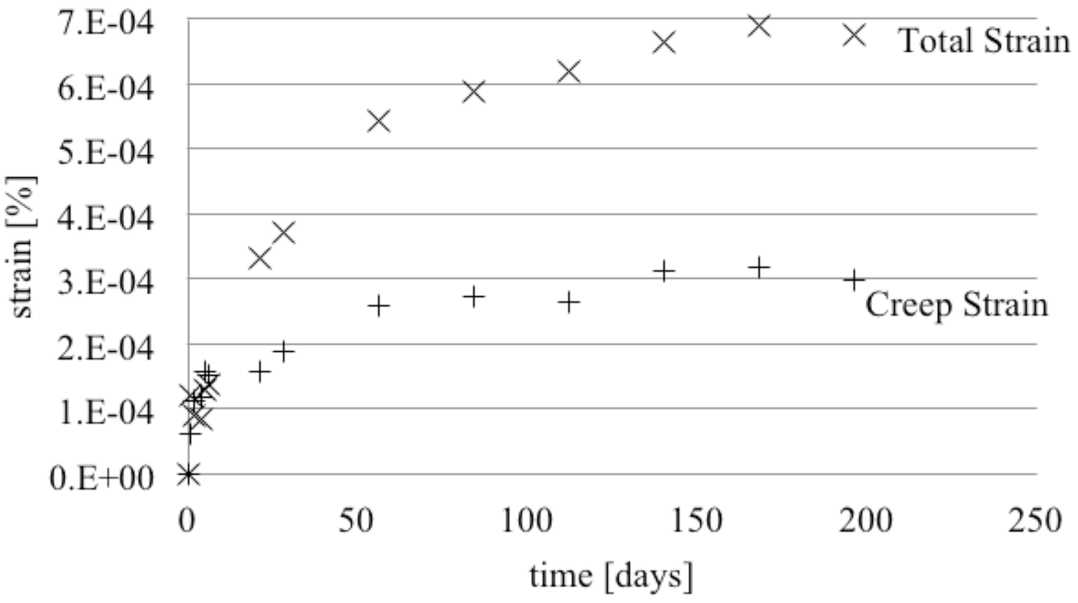

In Figure 6, Equation (3) is used to plot the creep coefficient using the upper and lower bound ultimate creep values for typical PCC. The PCC control specimens displayed typical behavior. The ultimate creep data appears to be well within the range of expected values for PCC of between C_u=1.30 and C_u=4.15. After 100 days of loading, the creep coefficient equaled 1.25, as compared to 0.9, the lower bound value for creep behavior.

Figure 6 shows that C_u for the GCC-2 specimens appears to be less than 1.0. Although data are presented for 200 days of loading, creep does not seem to be increasing significantly for successive measurements beyond the 100th day. The range defined by C_u=1.30 and C_u=4.15 on the charts denote the typical range of the creep coefficient for Portland cement concrete. The GCC is well below the lower end of this range, indicating that the creep behavior of GCC is significantly improved over the expected behavior of PCC.

Figure 6: GCC and PCC creep coefficient compared to the range of ultimate creep values for Portland cement concrete.

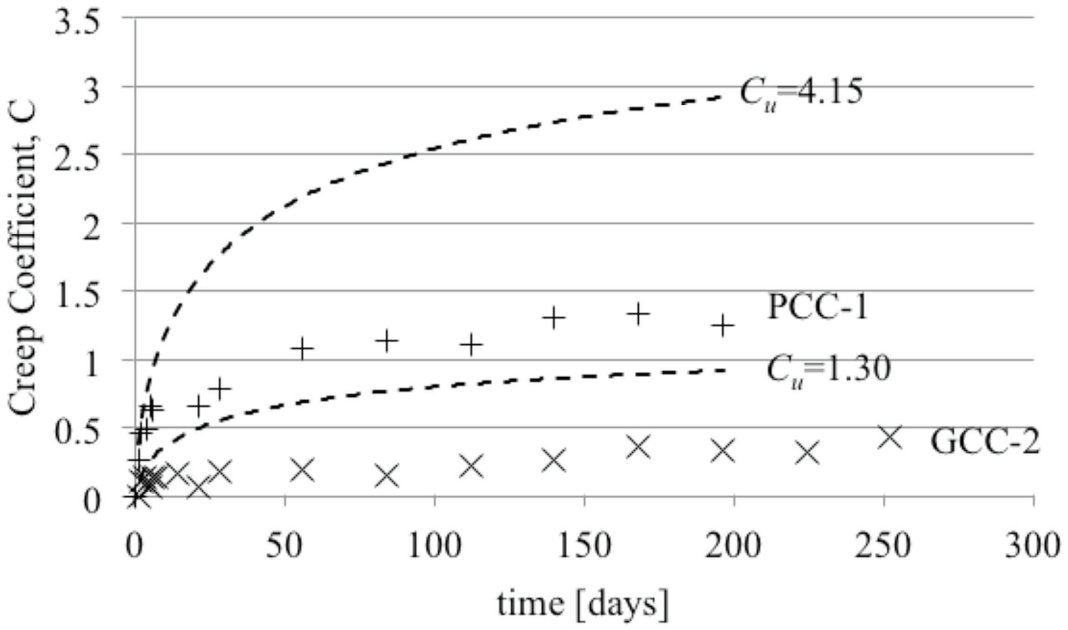

Shrinkage Measurement

In order to determine shrinkage experimentally, concrete is cured and aged under controlled environmental conditions that are set at temperature and humidity levels of interest. Generally, the environmental conditions used to establish baseline shrinkage magnitudes are 22.7°C (73°F) and 50% relative humidity, and these conditions were used in this study. General procedures for conducting shrinkage measurements are given by ASTM 157 (2008). 76mm x 76mm x 286mm (3”x3”x11.25”) concrete prisms are formed and outfitted with gage studs in each end.

GCC specimens for measurement of shrinkage were prepared using the mixing proportions given in Table 1. Data were collected for the shrinkage behavior of the three concrete mix types. Four prisms were prepared from each concrete mix. In order to not confound the results with processes that are not related to drying shrinkage, the PCC specimens were handled in accordance with ASTM 157 (2008). The specimens were removed from the molds after 24 hours, placed in lime-saturated water for 1 hour, and then an initial measurement was made. The specimens were stored in the lime water for a period of 28 days, and readings were made at 4, 7, 14, 28 and 56 days.

GCC materials were handled slightly differently from the ASTM procedures since these guidelines do not have provision for geopolymer cement concretes. The specimens were

consolidated in the forms by rodding and covered with plastic. Rather than removing the samples from the mold after 24 hours (as with PCC), they were allowed to age for two days. Following the aging period, they were cured at 75°C (167°F) for 48 hours. After removal from the forms, the GCC specimens were measured immediately with a length comparator and then stored for the duration of the test in the same environmental chamber as the one used for the PCC specimens.

Data was available for 224 days of post-curing shrinkage for PCC and GCC-2. Table 6 provides the average strain for each group of four prisms and Figure 7 illustrates the increase in shrinkage strain with time. The largest shrinkage strains were found in the PCC mix. Shrinkage increased rapidly between day 0 and day 28. The strains appear to be approaching 700 x 10^{-6} mm/mm (in/in), which is within the typical range for Portland cement concrete. Moist-cured Portland cement concrete has an average ultimate shrinkage strain of 800 x 10^{-6} mm/mm (in/in).

TABLE 6. Shrinkage test results.

Mixture	Microstrain at Day							
	0	4	7	14	28	56	112	224
PCC	0	-40	180	230	430	480	510	630
GCC-2	0	-	60	-	-	120	240	220

The GCC-2 concrete indicates a more gradual approach to an upper value of 240 x 10^{-6} mm/mm (in/in) at 112 days. Some data from cylinders created for creep testing was supplemented in Figure 7b, since the data from the shrinkage tests at days 4, 14 and 28 were strong outliers. The cylinders providing the supplementary data were stored in the same environmental chamber and were instrumented for precision measurements over a gage length of 203 mm (8”). The same shrinkage trends are seen in the cylinders as in the shrinkage prisms and the proximity of the data points along the curve in Figure 7b verifies the behavior in place of the missing measurements.

In order to use Equation (5) to estimate shrinkage in concrete, the terms α and f must be determined. As Equation (5) is simply a hyperbolic equation, reducing α below values of 1.0 will tend to steepen the ascending branch of the curve. Values of f affect how quickly the curve approaches the asymptotic value $(\varepsilon_{sh})_u$. Using a multi-parameter curve fitting tool in MathCAD, values for α and f were found to describe the behavior of the GCC-2 material. In the model $(\varepsilon_{sh})_u$ was taken to be 300 x 10^{-6}. With values of α=0.8 and f=0.9, the curve fits the data with R^2=0.952. A plot showing this curve is given in Figure 8.

GCC-2 concrete specimens tested for shrinkage resulted in lower strains at each time increment than comparison cylinders made from Portland cement concrete. Strains in the PCC batch were more than 200% of the strains found in both geopolymer mixes. For PCC the shrinkage strains appeared to approach 700 x 10^{-6} mm/mm (in/in), which is typical for moist cured PCC. For the GCC-2 batch, the limit appeared to be in the range of 300 x 10^{-6} mm/mm (in/in).

It is important to note that the test procedure is set-up to measure shrinkage in the GCC that occurred only after high temperature curing. However, it will be important to understand and predict any volume changes that occur in the GCC as it undergoes the aging process

Figure 7: Comparison of shrinkage in PCC-1 and GCC-2 specimens.

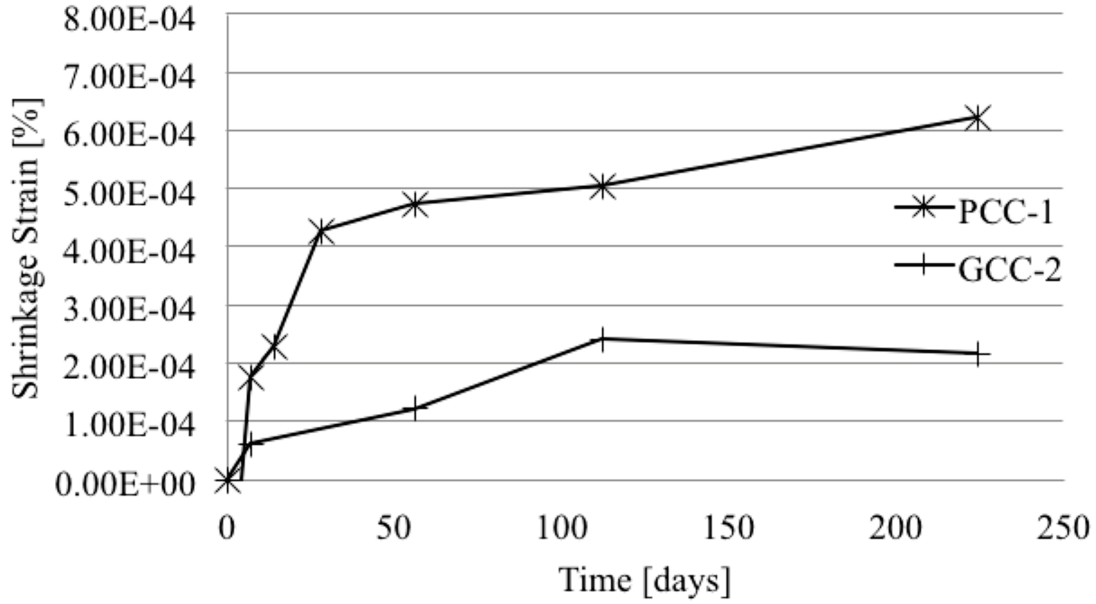

(A)

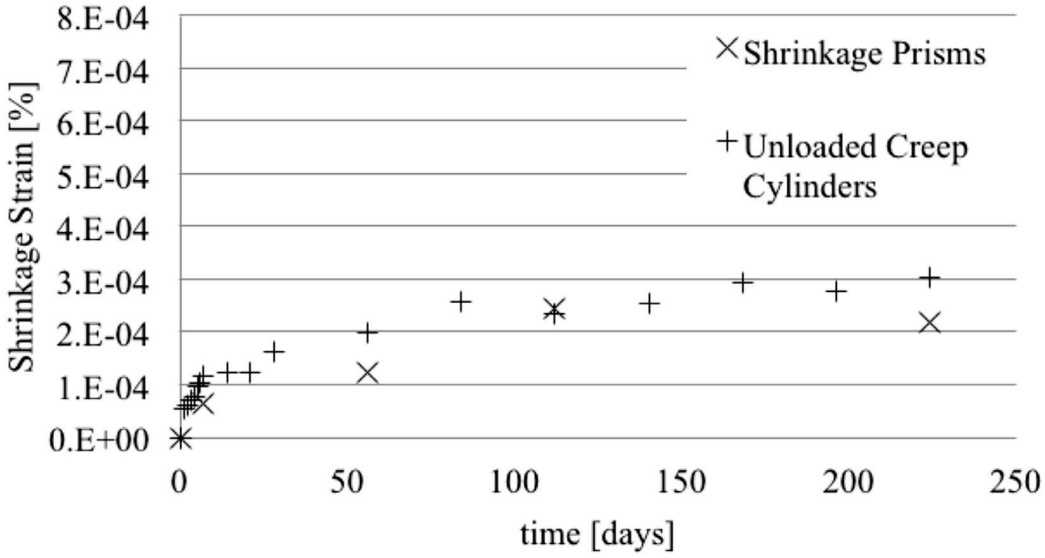

(B)

and the high temperature curing process. These changes could be attributable to both the action of water evaporation from pore spaces in the GCC as well as to the formation of polymeric bonds during the hardening phase. A technique to measure these strains would need to account for the thermal expansion that occurs during elevated temperature curing.

Shrinkage and creep phenomena observed in geopolymer materials during this study were both significantly lower in magnitude than in the Portland cement companion materials. Both phenomena are linked to processes involving water in Portland cement. Although full

Figure 8: Prediction of shrinkage of GCC using α=0.8 and f=0.9.

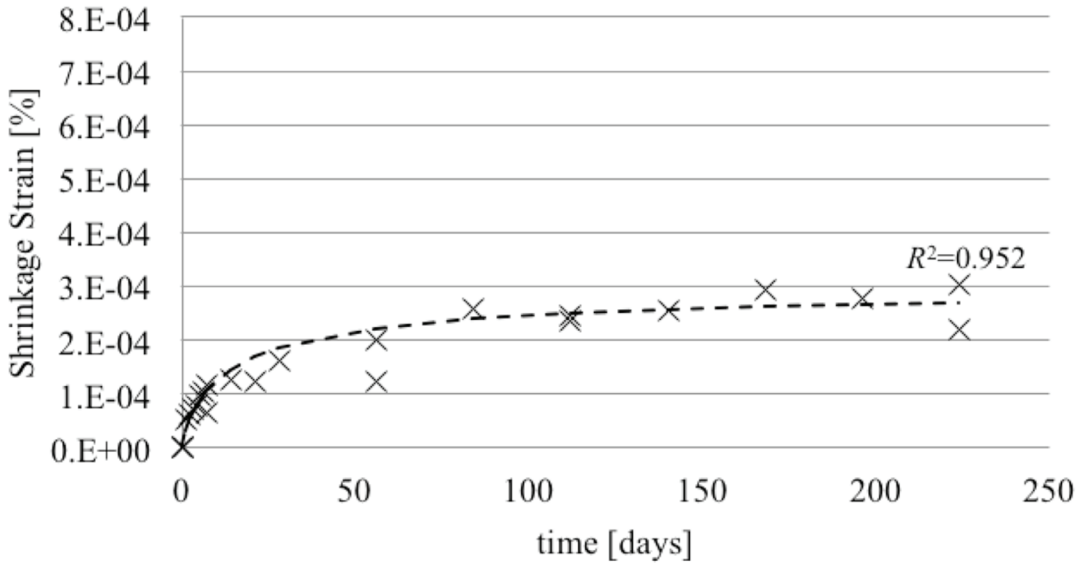

understanding of the shrinkage and creep mechanisms in GCC was beyond the scope of the research presented in this paper, one likely explanation of the observation is the very different role of water in GCC. The curing process of geopolymer does not involve hydration reactions. Most of the water present in the GCC is removed during the high temperature curing process, whereas, it is mostly present as pore water in PCC at the beginning of the curing process. As a result, much of the shrinkage that occurs in GCC materials may occur during the initial stages of curing when the mass is heated. Creep in Portland cement concrete is also known to occur in the presence of water. Water disrupts the van der Waals' forces that provide attraction between C-S-H hydration products and enables slippage between adjacent particles when the concrete is under stress. In GCC, the binder forms chemical bonds between particles and is not subject to disruption by water. Therefore, this mechanism of creep likely does not apply to GCC, although other processes, such as disjointing stresses caused by diffusion of pore water, likely do occur.

SUMMARY AND CONCLUSIONS

In order to enable wider-spread use of geopolymer materials in structural and infrastructure applications, design parameters related to strength and elastic properties of GCC must be established. Towards that goal, several samples of GCC materials were prepared and evaluated for their immediate compressive strength, tensile strength and modulus of elasticity. The results of these tests were used to correlate the splitting tensile strength and compressive elastic modulus with concrete compressive strength in order to establish an "indexed" relationship that can be used for estimation. GCC materials were prepared with two levels of alkalinity in the activating solution. The set of samples having the higher alkalinity solution also featured greater compressive strength due to increased ash dissolution. The effect of additional sample aging time, as well as sample curing time was most pronounced in the samples prepared with the higher alkalinity activating solution. Thus, it seems that in cases where greater compressive

strength is required, this may be achieved by using higher molarity activating solutions as well as by increasing the aging and curing times. However, given the chemical inputs to the activating solution, the most economical and sustainable means to increase compressive strength of samples may be to avail increased aging time, which does not require energy input. Further optimization of this process, combined with life cycle assessment of the alternatives, should be considered in follow-up research.

These studies have also determined that, as with PCC, the tensile strength characteristic of the concrete may be indexed to the compressive strength. In samples tested for this research, a correlation between compressive strength and the splitting tensile strength was found to have R^2=0.84. The splitting tensile strength of GCC samples tested was approximately 15% higher than PCC of a similar compressive strength. Because of the slightly greater tensile strength of GCC, prestressing for the objective of crack control may be effective at lower effective stresses than would be required for PCC.

The elastic modulus of the GCC was also evaluated and found to be correlated with compressive strength with R^2=0.94. The GCC's elastic modulus was slightly lower than that of PCC with similar compressive strength. For purposes of design, these results indicate that GCC would likely experience slightly greater elastic deformations than similarly loaded and equivalent strength PCC. However, long-term deformations would likely be slightly lower for the GCC.

Long term tests were also performed to observe the creep and shrinkage behavior of GCC. These tests indicated lower strains in the GCC related to shrinkage and creep than were realized for PCC of equivalent compressive strength. Analytical methods to determine the causes of the reduced volume changes were not applied because the fundamental mechanism in GCC is not yet known. The results indicate that there may be significant benefits to using GCC materials in precast-prestressed applications. The reduced susceptibility to volume changes would lead to lower loss of prestress over the lifecycle of the structure. This could lead to resilience and sustainability benefits by extending the service life of structures and making them less vulnerable to degradation.

These results indicate that GCC is a feasible material for structural concrete applications. This study has focused on concretes made from a limited number of batches of source materials and has evaluated the performance of concretes under controlled, laboratory conditions. In order to improve the quality of some of the results, as well as to increase confidence in some of the conclusions, subsequent studies should report on a greater variety of aggregate types, sizes and volumetric contents. It is also likely that the source and composition of the fly ash source materials and the chemistry of the activating solution would have a great impact on the mechanical characteristics of the concrete. Testing conducted at earlier and later concrete ages would help researchers understand the time-dependency of strength, elastic and volume change phenomena.

REFERENCES

ACI Committee 209 (2008). "Prediction of creep, shrinkage and temperature effects in concrete structures", American Concrete Institute.

ACI Committee 311 (2011). *Building code requirements for structural concrete: (ACI 318-11) and commentary (ACI 318R-11)*, American Concrete Institute, Farmington Hills, Mich.

ASTM (2002). "C469-02e1 Standard test method for static modulus of elasticity and poissons ratio of concrete in compression", ASTM International, West Conshohocken, PA.

ASTM (2002). "C512-02 Standard test method for creep of concrete in compression." ASTM International, West Conshohocken, PA.
ASTM (2004). "C496/C496M-04e1 Standard test method for splitting tensile strength of cylindrical concrete specimens", ASTM International, West Conshohocken, PA.
ASTM (2005). "C39/C39M-05e1 Standard test method for compressive strength of cylindrical concrete specimens", ASTM International, West Conshohocken, PA.
ASTM (2007). "C192 Standard Practice for Making and Curing Concrete Test Specimens in the Laboratory." ASTM International, West Conshohocken, PA.
ASTM (2008). "C 157 Standard test method for length change of hardened hydraulic-cement mortar and concrete." ASTM International, West Conshohocken, PA.
Azarbayjani, M., Futrell, B., Cecchi, V., Gentry, T., and Ebong, A. (2014). "The Road Map to the Integrated Design Process of a Net-Zero Energy Solar House: A Case Study of a Solar Decathlon Competition Entry." Journal of Green Building, 9(2), 20-37.
Branson, D. E. (1976). *Deformation of concrete structures*, McGraw-Hill, New York.
Diaz-Loya, E. I., Allouche, E. N., and Vaidya, S. (2011). "Mechanical properties of fly-ash-based geopolymer concrete." *ACI Materials Journal*, 108(3).
Fernández-Jiménez, A., and Palomo, A. (2005). "Composition and microstructure of alkali activated fly ash binder: Effect of the activator." *Cement and Concrete Research*, 35(10), 1984-1992.
Glukhovsky, V. D. (1959). *Soil silicates*, Gosstroyizdat, Kiev.
Hardjito, D., and Rangan, B. (2005). "Development and properties of low-calcium fly ash-based geopolymer concrete." Curtin University of Technology, Perth, Australia, 103 pages.
Johnson, N., *UQ building by Hassell collects six green stars from GBCA in infolink*. 2014, Cirrus Media: Australia.
Mikuni, A., Komatsu, R., and Ikeda, K. (2007). "Dissolution properties of some fly ash fillers applying to geopolymeric materials in alkali solution." *Journal of Materials Science*, 42(9), 2953-2957.
Mindess, S., Young, J. F., and Darwin, D. (2003). *Concrete*, Prentice Hall, Upper Saddle River, NJ.
Panagiotopoulou, C., Kontori, E., Perraki, T., and Kakali, G. (2007). "Dissolution of aluminosilicate minerals and by-products in alkaline media." *Journal of Materials Science*, 42(9), 2967-2973.
Panias, D., Giannopoulou, I. P., and Perraki, T. (2007). "Effect of synthesis parameters on the mechanical properties of fly ash-based geopolymers." *Colloids and Surfaces A: Physicochemical and Engineering Aspects*, 301(1-3), 246-254.
Sagoe-Crentsil, K., and Weng, L. (2007). "Dissolution processes, hydrolysis and condensation reactions during geopolymer synthesis: Part II. High Si/Al ratio systems." *Journal of Materials Science*, 42(9), 3007-3014.
Sindhunata, vanDeventer, J. S. J., Lukey, G. C., and Xu, H. (2006). "Effect of curing temperature and silicate concentration on fly-ash-based geopolymerization." 3559-3568.
Sun, P. (2005). "Fly ash based inorganic polymeric building material." Doctoral dissertation, Wayne State University.
Tempest, B (2010). "Engineering Characterization of Wste Derived Geopolymer Cement Concrete for Structural Applications." Doctoral dissertation, The University of North Carolina at Charlotte.
van Jaarsveld, J. G. S., and van Deventer, J. S. J. (1999). "Effect of the Alkali Metal Activator on the Properties of Fly Ash-Based Geopolymers." *Industrial & Engineering Chemistry Research*, 38(10), 3932-3941.
van Jaarsveld, J. G. S., van Deventer, J. S. J., and Lukey, G. C. (2002). "The effect of composition and temperature on the properties of fly ash- and kaolinite-based geopolymers." *Chemical Engineering Journal*, 89(1-3), 63-73.
Wight, J. K., Richart, F. E., and MacGregor, J. G. (2012). *Reinforced concrete : mechanics and design*, Pearson Prentice Hall, Upper Saddle River, N.J.